J. Cosmet. Sci., **69,** 305–313 (September/October 2018)

Hair Mechanical Anisotropy—What Does It Tell Us?

STEVEN BREAKSPEAR, BERND NOECKER, and
CRISAN POPESCU, *Kao European Research Laboratories, KAO Germany GmbH, Darmstadt D-64297, Germany (S.B., B.N., C.P.)*

Synopsis

Hair fibers were examined by atomic force microscopy, nanoindentation. By indenting along (longitudinal) and across (transversal) the fiber, we evaluated the Young's modulus and its dependence on the moisture content (relative humidity) of the environment. The ratio of the two values collected for Young's modulus, at a given relative humidity, is defined as the anisotropy index (*IA*) of the fiber and the acquired results give the evolution of the index of anisotropy with the relative humidity. The use of the model of composite materials allowed us to relate the anisotropy index to the fiber internal architecture. The evaluation of the results acquired on the components of the fiber, within the frame of this model, ultimately points to a possible micro-structure of exocuticle, hindered under usual circumstances by its heavy cross-linking and only noticeable when the absorbed moisture swells the surrounding network and annuls, in this way, its effect.

INTRODUCTION

Hair fibers' structural analysis reveals an intricate assembly of protein materials. Moving from the cortex (inside) of the fiber toward the periphery there are some highly ordered rod-like regions, keratin intermediate filaments (KIF), surrounded by keratin-associated proteins, cellular membrane complex, and other cellular remnants, all wrapped by flat cuticle cells (1). The cuticles themselves consist of subcomponents, namely the endo- and exocuticles.

Commonly, hair mechanics are evaluated by a tensile test, performed along the growth axis, and produce the well-known sigmoidal stress-strain curve (2). An impressive amount of work has been dedicated to analyzing this curve to extract as much information as possible about the hair subcomponents and their role in the overall architecture and behavior of hair (3,4). This method, however, provides information only along one direction and, in addition, lacks the required resolution for discriminating among the contributions of the fiber subcomponents.

Although the measurement of fiber torsion appears to provide a complementary picture of fiber mechanics, with the mechanical action taking place in a plane perpendicularly to

Address all correspondence to Crisan Popescu Crisan.Popescu@kao.com.

the long axis (5), this method also lacks the ability to distinguish among the fine subcomponents but may offer data on cuticle contribution (6).

Atomic force microscopy (AFM), since its emergence (7), has enabled higher spatial resolution. This has made AFM the ideal tool for investigating the mechanics of the hair subcomponents (8,9). Moreover, AFM nanoindentation is able to measure the mechanics of the hair subcomponents in any direction. Acquiring the mechanical response of the same subcomponent along different axes has, so far, not been performed, however, by other investigators. This study aims to explore this aspect, expecting that such data provide new hints about hair architecture.

MATERIALS AND METHODS

HAIR SAMPLES

Virgin hairs were collected from a European female, close to the root, and washed. The washing process consisted of sonication of the hairs in 1% aqueous sodium dodecylsulphate (50 cm^3) for 1 min, sonication in deionized and UV irradiated water (50 cm^3) for 1 min, followed by rinsing with copious amounts of the same and, finally, gentle drying under a stream of nitrogen.

AFM

All AFM measurements were performed in a closed cell under controlled relative humidity, RH, which can be adjusted to the intended value ±1%, and a temperature of 25 ± 1°C, using a MFP-3D Scanning Probe Microscope (Asylum Research, Santa Barbara, CA). Samples were equilibrated for 1 h before each measurement.

Fibers were embedded in Epon 812 resin (TAAB Laboratories Equipment Ltd., Aldermaston, Berkshire, UK) and, after curing, excess epoxy material was removed from around the embedded hair with a razor blade, and the top 2 mm of the resin block, containing the hair sample, was severed and mounted on a steel AFM sample stub with silver paint, ensuring that the hair samples were perpendicular (for cross sections) or parallel (for longitudinal sections) to the sample stub. Smooth hair sections were then exposed by ultramicrotome (Reichert Ultracut N Ultramicrotome, Wien, Austria), using a diamond knife (Ultra 45, Diatome Ltd., Biel, Switzerland).

Force curves and corresponding images on hair sections were acquired using a rectangular silicon nitride cantilever of length and nominal spring constant, k, 160 μm and 42 N m^{-1}, respectively (Olympus Corp., Tokyo, Japan). The anatomy of force curves and the extraction of nanoindentation data have been described elsewhere (10).

To overcome the uncertainty in knowing the tip radius, necessary for evaluating the samples elastic moduli, five polymer samples, listed in Table I, with known Young's moduli, E, and Poisson's ratios, υ, were measured, as a means of indirectly calibrating the AFM system (11).

Approximately, 2 × 2 mm pieces of each polymer were embedded in Epon 812 resin, mounted, and cut by ultramicrotome, in the same manner as for the hair samples.

Table I
Polymers Used for Calibration (BASF SE, Ludwigshafen, Germany)

Polymer	Young's modulus, GPa	Poisson's ratio, ν
Low density polyethylene	0.2	0.43
High density polyethylene	1.3	0.46
Polypropylene	1.45	0.40
Polycarbonate	2.4	0.37
Polymethyl methacrylate	3.2	0.375

To acquire force curves, the AFM was operated in indentation mode, using a low trigger value (0.01 V) to detect the sample surface. Then an indentation of fixed depth (maximum 25 nm, indentation rate 50 nm s^{-1}) was performed. Using the Force Map mode of the AFM it was possible to obtain 196 force curves from 14 × 14 arrays, on 2 × 2 μm regions of the cortex of the hairs. A similar process was carried out for the polymer standards. For the cuticle regions, manual selection of the position of each force curve using the AFM software was performed. Using the polymer reference samples and a nominal tip radius, R, of 10 nm for calculation, a calibration plot was constructed, which could then be used to determine elastic modulus values for the hair samples. All indentation data were individually handled using a Microsoft Excel spreadsheet for curve fitting, using the Hertz model for a spherical indenter (12), where the applied force, F, and the indentation depth, h, are related to the reduced modulus, E^*, by

$$F = \frac{4 \cdot E^* \cdot R^{0.5} \cdot h^{1.5}}{3} \tag{1}$$

Values of the Young's modulus, E, were obtained from E^* by evaluation with the Poisson's ratios, as per equation (2) (13).

$$\frac{1}{E^*} = \frac{1-\nu^2_{\text{sample}}}{E_{\text{sample}}} + \frac{1-\nu^2_{\text{tip}}}{E_{\text{tip}}} \tag{2}$$

For soft samples, where E_{sample} is considerably lower than E_{tip}, the second term in equation (2) can be ignored. A value of 0.5 for the Poisson's ratio was assumed for hair, in line with previously reported measurements on wool (14).

THE MODEL

A simple but widely used model, the 2-phase model, regards the cortex of hair as a composite material consisting of rods (the KIF) arranged parallel to the growing axis of the fiber and contained in a less ordered matrix (15). This model allows for describing the Young's moduli acquired along axial and transverse axes, respectively, by the "rule of mixtures" for composites (16,17).

The orientations of the nanoindentation measurements are illustrated in Figure 1, for (a) cross sections, and (b) for longitudinal sections.

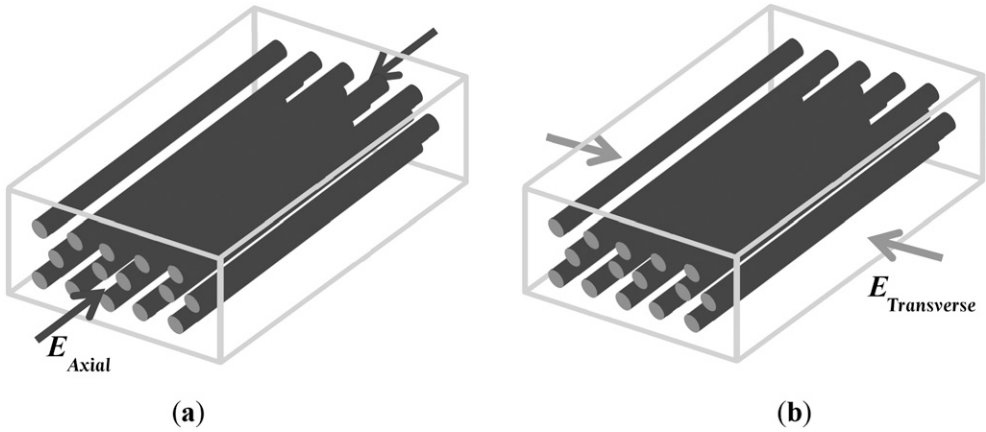

Figure 1. The indenting on cross-section (A) and on longitudinal section (B) of a hair fiber schematically designed as a rod-matrix composite material.

This allows writing, for the axial and transverse moduli, the equations:

$$E_{\text{Axial}} = E_{\text{ROD}} \cdot x_{\text{ROD}} + E_{\text{Matrix}} \cdot \left(1 - x_{\text{ROD}}\right), \tag{3}$$

$$E_{\text{Transverse}} = E_{\text{ROD}} \cdot E_{\text{Matrix}} \Big/ \left[E_{\text{Matrix}} \cdot x_{\text{ROD}} + E_{\text{ROD}} \cdot \left(1 - x_{\text{ROD}}\right)\right], \tag{4}$$

where E_{ROD} and E_{Matrix} are the Young's moduli of rods and of the matrix, respectively, and x_{ROD} is the percentage contribution of rods to the total fiber:

$$x_{\text{ROD}} = m_{\text{ROD}} \Big/ \left(m_{\text{fibre}} + m_{\text{moisture}}\right) \tag{5}$$

The percentage contribution of rods to the total fiber, equation (5), includes the changes due to sorption-desorption of moisture. This introduces the contribution of the relative humidity and temperature of the surrounding environment to the mechanical properties (18,19).

As suggested qualitatively by Figure 1A and B, and quantitatively by equations (3) and (4), the hair fibers should exhibit an asymmetrical behavior, i.e., they have anisotropic elasticity. For characterizing the anisotropy we define an index, termed "index of anisotropy", *IA*, by taking the ratio of the two measurable axial and transverse Young's moduli:

$$IA = \frac{E_{\text{Axial}}}{E_{\text{Transverse}}} = \frac{\left[E_{\text{ROD}} \cdot x_{\text{ROD}} + E_{\text{Matrix}} \cdot \left(1 - x_{\text{ROD}}\right)\right]\left[E_{\text{Matrix}} \cdot x_{\text{ROD}} + E_{\text{ROD}} \cdot \left(1 - x_{\text{ROD}}\right)\right]}{E_{\text{ROD}} \cdot E_{\text{Matrix}}} \tag{6}$$

Defining the ratio of the Young's moduli of rods to those of matrix:

$$Y = E_{\text{ROD}} \big/ E_{\text{Matrix}} \tag{7}$$

the index of anisotropy can be further expressed as:

$$IA = \frac{E_{\text{Axial}}}{E_{\text{Transverse}}} = x_{\text{ROD}} \cdot \left(1 - x_{\text{ROD}}\right) \cdot \frac{\left(Y - 1\right)^2}{Y} + 1 \tag{8}$$

As defined by equation (8), the index of anisotropy is greater than 1; it equals unity only for the isotropic material, i.e., for keratin fibers having either no rods ($x_{ROD} = 0$), only rods ($x_{ROD} = 1$), or equal values for Young's modulus of the rods and of the matrix ($Y = 1$).

The definition of index of anisotropy, as a ratio of AFM nanoindentation measurements, along and transverse to fiber axis has the particular advantage of avoiding any supposition on the Poisson ratio for fibers required by equation (2) for calculating the absolute value of the measured Young's modulus. Indeed, from equation (2):

$$\frac{E_{\text{Axial}}}{E_{\text{Transverse}}} = \frac{E^*_{\text{Axial}}}{E^*_{\text{Transverse}}} \cdot \frac{E_{\text{tip}} - E^*_{\text{Transverse}} \cdot \left(1 - \upsilon^2_{\text{tip}}\right)}{E_{\text{tip}} - E^*_{\text{Axial}} \cdot \left(1 - \upsilon^2_{\text{tip}}\right)} \approx \frac{E^*_{\text{Axial}}}{E^*_{\text{Transverse}}}, \tag{9}$$

where $E^*_{\text{Axial, Transverse}}$ are the AFM-measured Young's moduli along the two directions and the value of Young's modulus of the tip, E_{tip}, is much larger than that of the soft material (hair). As per equation (9), the index of anisotropy can be extracted directly from AFM nanoindentation measurements performed on cross sections and on longitudinal sections (the ratio of the two acquired Young's moduli).

Equations (8) and (9) relate the measured axial and transverse moduli to the amount of rods of the composite material and to the ratio of rod-to-matrix Young's moduli. The theoretical dependence of the index of anisotropy on the percentage of rods is shown in Figure 2A. The graph of Figure 2B takes into account that the percentage of rods (KIFs) of the hair fiber is below 50% (20) and that this percentage decreases with increasing moisture absorption (increasing relative humidity).

For the sake of simplicity, we neglect several factors, which may affect slightly the anisotropy, namely the following: the angle of KIFs, taken in the present work as 0°; any tilting of KIFs with increasing moisture absorption; the contribution of the interphase, the region of links between KIFs and Matrix (21); and of other subcomponents of keratin fibers (22).

RESULTS AND DISCUSSION

AFM nanoindentation measurements were performed on several areas of the hair, both on cross-sectional and on longitudinal section, for cortex, exo- and endocuticle. The relative

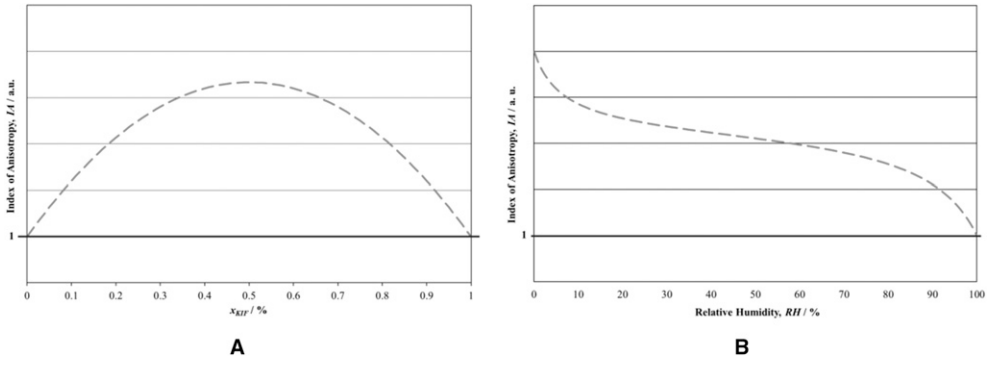

Figure 2. (A) Theoretical evolution of the index of anisotropy equation (8) with percentage of rods of the composite material. (B) Theoretical evolution of the index of anisotropy of Hair fiber with increasing Relative Humidity. The horizontal line at one is the 'isotropic line' for an isotropic material.

humidity, *RH*, during each indentation experiment was adjusted and controlled, to cover the range between 8% and 92%.

The values calculated, from equation (8), for the index of anisotropy of cortex (Figure 4A) do not appear to follow the shape suggested in Figure 2B, for moisture influencing only the percentage of rods (KIFs) of the cortex. This led us to consider that moisture, being absorbed only by matrix, affects the Young's modulus by breaking of hydrogen bonds and, in this way, affecting the rods-to-matrix moduli ratio, *Y* equation (7). The dotted line in Figure 4A plots the theoretical values of the model developed to account for the hydrogen bonds participation to the Young's modulus of the matrix (23):

$$E_{\text{Matrix}} = k\left(1 - \text{cortex moisture content}\right)^{1/3} + 0.2 \tag{10}$$

Figure 4B illustrates a striking result; namely that the exocuticle deviates from isotropic behavior (from $IA = 1$ line), when relative humidity goes beyond 60%–70% and the effect of relative humidity (dotted line) appears to match fairly well the experimental data. In other words, Figure 4B indicates that the exocuticle exhibits an internal composite structure when enough absorbed moisture allows its release from the otherwise isotropic, heavily cross-linked, environment.

Moreover, the values for the indices of anisotropy of exocuticle fall below one, which is at odds with our definition in equation (8); requiring the ratio of axial to transverse moduli to be greater than one. We interpret this behavior by assuming that in the case of exocuticle the orientation of its presumptive rods is perpendicular to the fiber growing axis and, likewise, to those of the KIFs of cortex.

The experimental results acquired for endocuticle (see Figure 4B), on the other hand, suggest a fair isotropic behavior of this layer over the range of relative humidity. This is in line with the knowledge of the low cross-linked structure of endocuticle (9).

Summing up the mechanical results, we hypothesize that exocuticle behave as a heavily cross-linked composite layer, keeping the rods in an isotropic tight arrangement until moisture content of the Cuticle is high enough (*RH* greater than 60%…70%) to allow the manifestation of the rods. The rods of the exocuticle appear to lie perpendicularly to the KIFs of cortex, i.e., perpendicularly to the growing axis of the fiber, very much similar

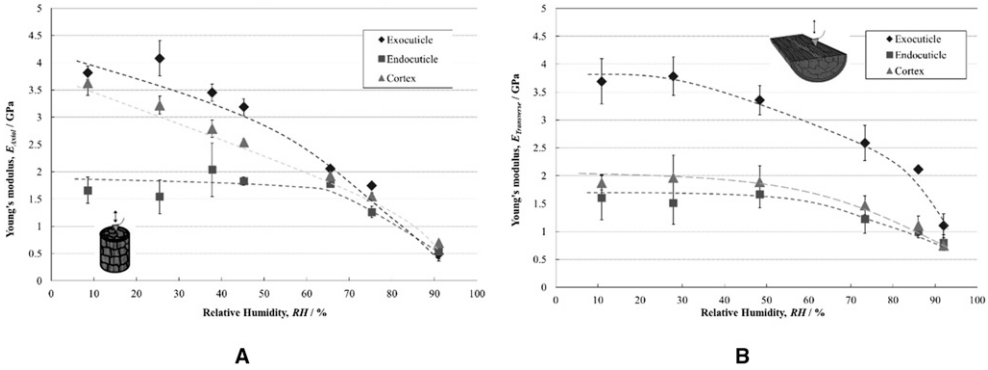

Figure 3. The evolution of axial (A) and transverse (B) Young's moduli for cortex, exo- and endocuticle with relative humidity. The dotted lines are for eye guidance.

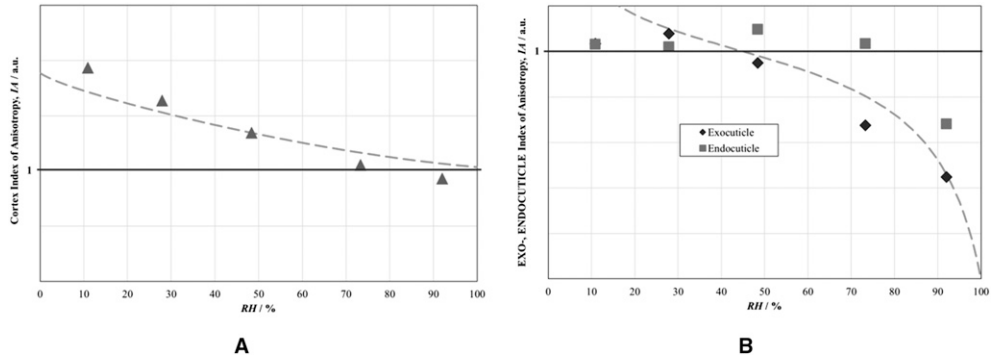

Figure 4. Evolution of index of anisotropy, *IA*, of (A) cortex and (B) exo- and endocuticle of the hair calculated from values of axial and transverse elastic moduli measured at increasing relative humidity, *RH*, and shown in Figure 3A and B. The dotted lines are the plots of the theoretical models. The horizontal line at one is the 'isotropic line'.

to the arrangement of alpha-keratins in the intermediate plate of the nails (24). Figure 5 illustrates these details.

It is worth mentioning that such an arrangement of exocuticle rods, combined with those of the KIFs in the cortex, provides the fiber with a greater mechanical stability and may explain why external mechanical or chemical insults to the fiber lead to breaking of the scales horizontally rather than longitudinally (25).

At this stage, we assume the proposed rods to exist in the cuticle layers as non-regular intermediate filaments, and the architecture of the layers as sketched in Figure 6.

CONCLUSIONS

Using AFM nanoindentation of hair fiber cross and longitudinal sections, we have evaluated for the first time, the mechanical anisotropy of a keratin fiber. Voigt and Reuss models were successfully used for calculating the behavior of the fiber as an ideal composite material made of rods (KIFs) and matrix, and the experimental results of virgin hair fibers matched fairly well to the theory.

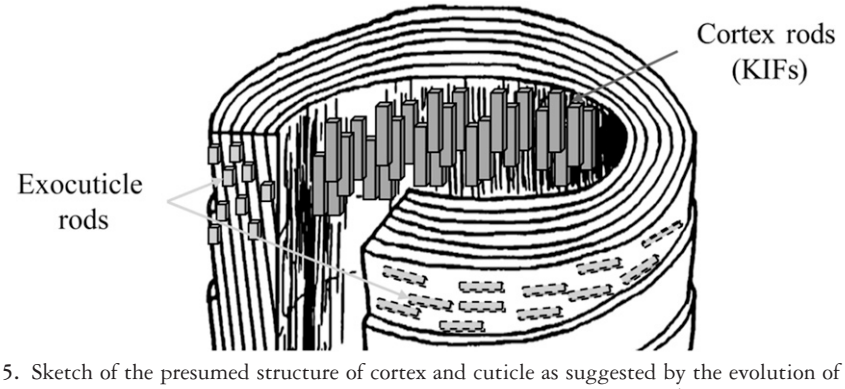

Figure 5. Sketch of the presumed structure of cortex and cuticle as suggested by the evolution of index of anisotropy, *IA*, of the subcomponents with Relative Humidity, *RH*, as in Figure 4.

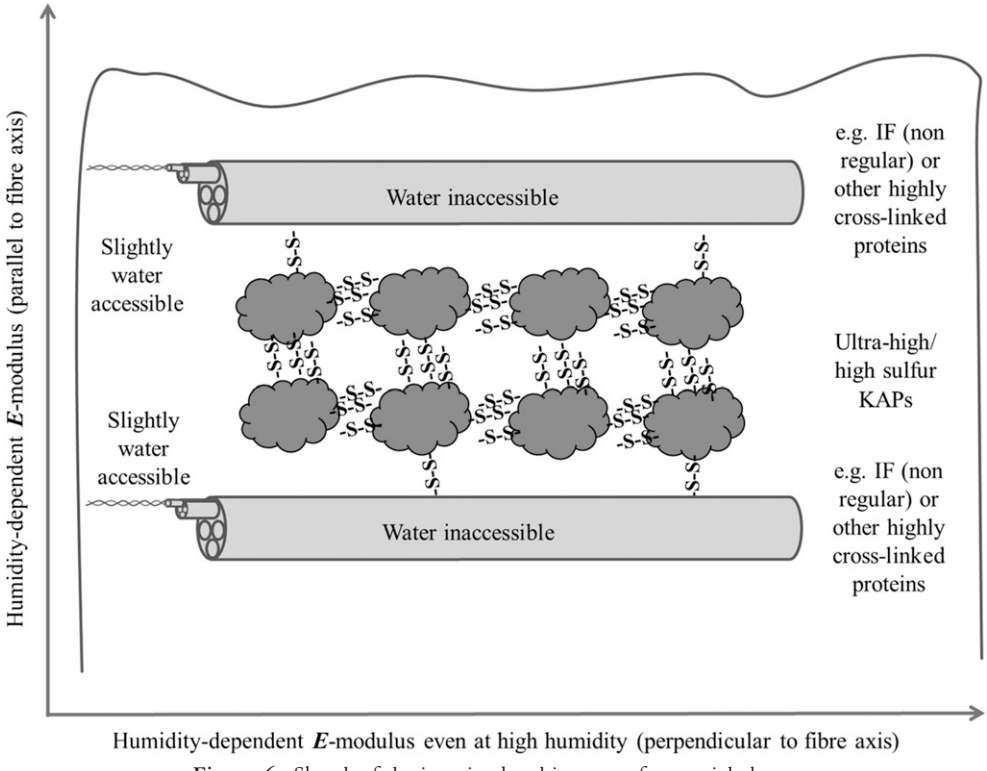

Figure 6. Sketch of the imagined architecture of exocuticle layer.

Applying the models further to the cuticle components (exo- and endocuticle) and using the "index of anisotropy," *IA*, introduced by equation (8), the experimental results indicated that, for high values of relative humidity, when the cuticle layers are swollen enough, a probable composite structure of exocuticle, masked so far by the heavy cross-linking of the environment, manifests. The rods reinforcing the exocuticle composite structure appear to be oriented perpendicularly to the fiber-growing axis, in what we consider to be an attempt by nature to ensure a balanced design for a fiber able to withstand various directional stresses.

REFERENCES

(1) C. Popescu and H. Hoecker, Hair—the most sophisticated biological composite material, *Chem. Soc. Rev.*, **36**, 1282–1291 (2007).
(2) C. Popescu and H. Hoecker, Cytomechanics of hair: basics of the mechanical stability, *Int. Rev. Cell Mol. Biol.*, **277**, 137–156 (2009).
(3) J. W. S. Hearle, A critical review of the structural mechanics of wool and hair fibres, *Int. J. Biol. Macromol.*, **27**, 123–138 (2000).
(4) M. Feughelman, Natural protein fibres, *J. Appl. Polym. Sci.*, **83**, 489–507 (2002).
(5) H. Bogaty, Torsional properties of hair in relation to permanent waving and setting, *J. Soc. Cosmet. Chem.*, **18**(10), 575–590 (1967).
(6) L. J. Wolfram and L. Albrecht, Torsional behavior of human hair, *J. Soc. Cosmet. Chem.*, **36**(1), 87–99 (1985).
(7) G. Binnig and C. F. Quate, Atomic force microscope, *Phys. Rev. Lett.*, **56**(9), 930–933 (1986).

(8) S. D. O'Connor, K. L. Komisarek, and J. D. Baldeschwieler, Atomic force microscopy of human hair cuticles: a microscopic study of environmental effects on hair morphology, *J. Invest. Dermatol.*, **105**(1), 96–99 (1995).
(9) J. A. Swift and J. R. Smith, Microscopical investigations on the epicuticle of mammalian keratin fibres, *J. Microsc.*, **204**(3), 203–211 (2001).
(10) J. R. Smith, S. Breakspear, R. J. R. Fletcher, and S. A. Campbell, AFM in surface finishing: part IV. Force–distance curves, *Trans. Inst. Met. Finish.*, **83**, 63–67 (2005).
(11) C. A. Clifford and M. P. Seah, Quantification issues in the identification of nanoscale regions of homopolymers using modulus measurement via AFM nanoindentation, *Appl. Surf. Sci.*, **252**, 1915–1933 (2005).
(12) H. Hertz, Ueber die berührung fester elastischer koerper, *J. Reine Angew. Math.*, **92**, 156–171 (1881).
(13) K. L Johnson, Contact Mechanics (Cambridge University Press, Cambridge, 1985).
(14) J. P. Caldwell and W. G. Bryson, Elastic modulus mapping of the wool fibre cellular structure by atomic force microscopy., Proc. 11th Int. Wool Res. Conf., Leeds, UK, 2005.
(15) M. Feughelman, A two-phase structure for keratin fibers, *Textil. Res. J.*, **29**, 223–228 (1959).
(16) W. Voigt, Ueber die beziehung zwischen den beiden elasticitätsconstanten isotroper körper, *Ann. Phys.*, **274**, 573–587 (1889).
(17) A. Reuss, Berechnung der fließgrenze von mischkristallen auf grund der plastizitätsbedingung für einkristalle, *Z. Angew. Math. Mech.*, **9**, 49–58 (1929).
(18) R. L. D'Arcy and I. C. Watt, Analysis of sorption isotherms of non-homogeneous sorbents, *Trans. Faraday Soc.*, **66**, 1236–1245 (1970).
(19) I. C. Watt and R. L. D'Arcy, Water-vapour adsorption isotherms of wool, *J. Text. Inst.*, **70**, 298–307 (1979).
(20) M. Spei and R. Holzem, Thermoanalytical determination of the relative helix content of keratins, *Colloid Polym Sci.*, **267**, 549–551 (1989).
(21) D. Istrate, C. Popescu, M. Er Rafik, and M. Möller, The effect of pH on the thermal stability of fibrous hard alpha-keratins, *Polym. Degrad. Stabil.*, **98**, 542–549 (2013).
(22) M. Kadir, X. Wang, B. Zhu, J. Liu, D. Harland, and C. Popescu, The structure of the "amorphous" matrix of keratins, *J. Struct. Biol.*, **198**, 116–123 (2017).
(23) S. Breakspear, B. Noecker, and C. Popescu, Relevance and evaluation of hydrogen bond contribution to the mechanics of hard alpha-keratin fibres, *Chem. Phys. Lett.*, (2018) (submitted).
(24) J. C. Garson, F. Baltenneck, F. Leroy, C. Riekel, and M. Mueller, Histological structure of human nail as studied by synchrotron X-ray microdiffraction, *Cell Mol. Biol.*, **46**(6), 1025–1034 (2000).
(25) M. Gamez-Garcia, Cuticle decementation and cuticle buckling produced by Poisson contraction on the cuticular envelope of human hair, *J. Soc. Cosmet. Chem.*, **49**(4), 213–222 (1998).